Quantifying individual base stacking energies with the Centrifuge Force Microscope

Jibin Abraham Punnoose, Kevin J. Thomas , Arun Richard Chandrasekaran, Javier Vilcapoma, Andrew Hayden, Thomas Banco, Ken Halvorsen

The RNA Institute, University at Albany, State University of New York, Albany, NY 12222, USA.

Correspondence to: khalvorsen@albany.edu

Abstract

DNA is stabilized by inter-strand base pairing and intra-strand base stacking. Untangling these energy contributions is challenging, but has implications for understanding biological processing of DNA, and for many aspects of biotechnology including drug discovery, molecular modeling and DNA nanotechnology. Here, we developed novel DNA constructs and performed single molecule experiments using a custom Centrifuge Force Microscope (CFM) to probe energetics of base stacking interactions between single bases. Collecting rupture statistics from over 30,000 single-molecule tethers, we quantified 10 unique base stacking combinations and 4 modified nucleotides. For canonical bases, we found stacking energies strongest for purines (G|A at -2.3 ± 0.2 kcal/mol) and weakest for pyrimidines (C|T at 0.4 ± 0.1 kcal/mol). Among hybrid stacking with modified nucleotides, only a bulky fluorophore modification reduced stacking energy while phosphorylated, methylated, and RNA bases had little effect. We demonstrate the implications of the work with two biotechnology applications: using interfacial base stacks to tune the stability of a DNA tetrahedron, and to alter the kinetics of enzymatic ligation. These results provide new insights into fundamental DNA interactions that are critical in biology and biotechnology.

Introduction

DNA is the genetic material for all known living organisms. As a biopolymer, it is remarkable in its ability to efficiently carry genetic information, and for material properties that provide high overall stability and yet still allow biological manipulation. These properties are illustrated by the fact that ancient genomes have been recovered from DNA over 100,000 years old [1], and yet normal biological processes routinely manipulate DNA to unwind, split, and recombine. These features of DNA are governed primarily by two forces, base pairing between two complementary strands and coaxial base stacking between adjacent bases. Relatively small binding energies of individual bases enable biological manipulation at the single base level, while cumulative effects of hundreds to millions of bases ensure high overall stability.

Base pairing interactions are generally considered to play the dominant role in DNA and RNA material properties, causing base stacking interactions to be sometimes overlooked. However, base stacking interactions are essential for normal biological processes, for nucleic acid binding drugs including chemotherapeutics, and for many biotechnology applications. One interesting example is a minimal RNA kissing complex, which has only 2 canonical base pairs but exhibits unusually high mechanical stability similar to a ~10 bp duplex [2]. Molecular dynamics simulations and single-molecule work attributed the stability to base stacking interactions [3,4]. Indeed, base stacking is critical to biological processes including DNA replication [5,6], RNA polymerization [7], and formation and management of G-quadruplexes in telomeres [8,9]. Base stacking is also thought to be critical for supramolecular assembly of nucleobases in pre-biotic RNA as part of the RNA world hypothesis [10,11]. Stacking also effects drug development; many DNA and RNA binding drugs are small molecule intercalators which rely on stacking interactions to disrupt a multitude of diverse diseases

including cancers, viral infections, Myotonic dystrophy, and Parkinson's disease [12-14]. Synthetic base analogs such as LNA [15] and universal bases [16] partly rely on modified base stacking interactions, as does a DNA helix engineered with expanded size and stability [17]. The formation of synthetic DNA structures can rely heavily on base stacking, including DNA polyhedra [18], DNA crystals [19], and DNA liquid crystals [20], with some designs that assemble into 2D lattices using only blunt end stacking interactions [21,22].

Measuring base stacking is challenging due to the small energies, the difficulty in disentangling base pairing and base stacking contributions, and experimental limitations. Early studies used thermal melting spectrophotometry with different terminal overhanging ends to resolve these effects [23,24]. More recent direct experimental studies of stacking interactions used polyacrylamide gel electrophoresis (PAGE) gel assays of nicked dsDNA to quantify pairs of stacking interactions [25,26], or optical tweezers to monitor binding and unbinding of DNA nanobeams with terminal stacking interactions [27]. These studies have made immense contributions to our knowledge, but their design and experimental constraints have still precluded the measurement of base stacking between two individual bases rather than pairs of bases. This has prevented knowing stacking energies between an A and G, for example, because previous measurements also included stacking energies between the paired bases (T and C in this example).

Here we set out to directly measure individual base stacking interactions at the single molecule level. Single-molecule pulling techniques can apply biologically relevant picoNewton-level forces to individual molecules, and have been indispensable for the study of biomolecules including folding dynamics and mechanisms of biomolecular interaction [28]. Common single-molecule methods that apply force include optical and magnetic tweezers and atomic force microscopy (AFM). We expanded the single-molecule toolkit with the development of the Centrifuge Force Microscope (CFM), a high-throughput technique that combines centrifugation and microscopy to enable many single-molecule force-clamp experiments in parallel [29]. We have made several iterations to improve the technique, notably enabling single-molecule manipulation with a benchtop centrifuge [30-32], and other groups have advanced the technique as well [33,34]. The high throughput nature of the CFM makes it well suited to collect data from thousands of pulling experiments for a comprehensive assessment of individual base stacking interactions.

Combining the high-throughput CFM with novel DNA construct design enabled quantitative probing of individual base stacking interactions. We quantified base-stacking energies of 10 unique base combinations ranging from -2.3 ± 0.2 kcal/mol (G|A stack) to -0.4 ± 0.1 kcal/mol (C|T stack) with purines generally contributing more than pyrimidines. Stacking energy was not affected by phosphorylation, methylation, or substitution by an RNA nucleotide, but was reduced by a bulky fluorophore modification. Our detailed assessment of base stacking led us to explore the impacts of base stacking in DNA nanotechnology and molecular biology. We manipulated base stacking interactions in a DNA tetrahedron and in an enzymatic ligation reaction and altered the structural stability and reaction kinetics, respectively. Our work represents the first comprehensive picture of individual base stacking interactions, and provides concrete examples of how such knowledge can be applied.

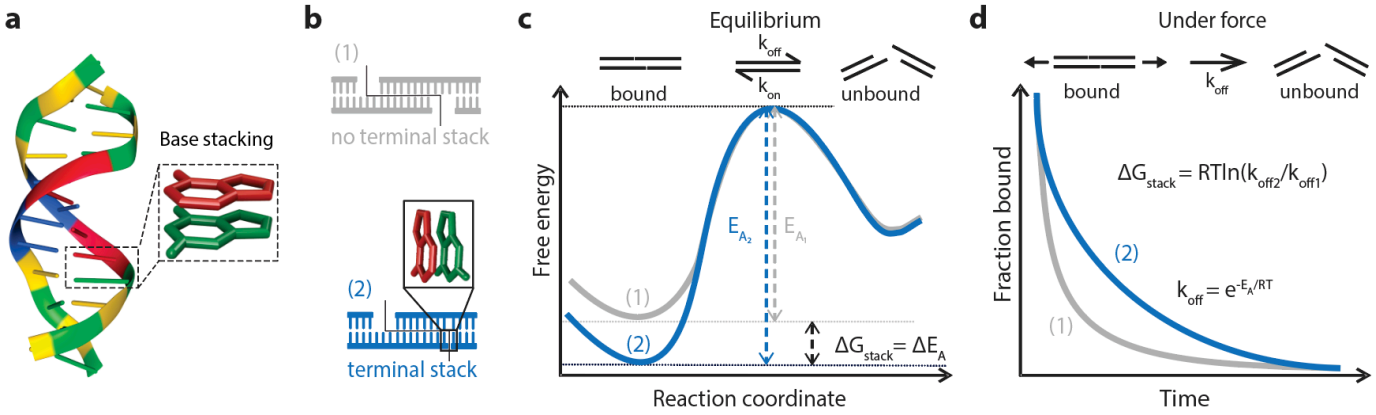

***Figure 1**: **Conceptual overview**.* (a) Model of a DNA duplex [35] with enlarged frame showing stacked adjacent bases. (b) Design of two duplexes differing by a single base stacking interaction. (c) Free-energy diagram of a DNA duplex with and without a terminal base stack. The base stack primarily increases the activation energy, with the difference representing the free energy of the single terminal base stack. (d) External force lowers the activation barriers and prevents rebinding, causing exponential dissociation that can be experimentally measured and used to calculate stacking free energy.

Results

Premise of experimental design

Base stacking interactions (Fig. 1a) are relatively weak on the order of ~1 kcal/mol, making the measurement of individual stacking interactions challenging. To address this, we considered the design of two duplexes that are weakly held together by identical base pairing but differ by presence or absence of a terminal base stack (Fig. 1b). This terminal base stack strengthens the interaction and lowers the energy of the bound state (Fig. 1c). The application of external force shifts the process out of equilibrium, allowing only the bound to unbound transition. Measurement of dissociation kinetics can then be used to determine the effect of a single terminal base stack (Fig. 1d). This design allows for flexibility in the overall experimental time scale by control of both the design of the base pairs in the central duplex and by the magnitude of the externally applied force. Building from previous work where we resolved the energy difference of a single nucleotide polymorphism [32], we hypothesized that properly designed single-molecule pulling experiments could resolve individual base stacking interactions.

To enable high throughput single-molecule pulling experiments, we used a custom designed CFM. The CFM is essentially a microscope that can be centrifuged, providing a controlled force application to single-molecule tethers, coupled with video microscopy imaging that can track individual tethers during the experiment (Fig. 2a). Using advances in 3D printing, cameras, and wireless communication electronics we recently integrated the microscope into a bucket of a standard benchtop centrifuge (Fig. 2b). We achieved live streaming of microscopy images during centrifugation by WiFi communication with an external computer that controls both the centrifuge and the camera through custom Labview software (Fig. 2c). During a typical experiment, we observe tens to hundreds of tethered microspheres in a full field of view at 40x magnification (Fig. 2d). As the centrifuge spins, force is applied to a DNA construct tethered between a glass slide and microspheres, forcing dissociation of a duplex over time and causing the microspheres to disappear from view (Fig. 2e). Each microsphere is monitored to track individual dissociation events (Fig. 2f), which are used to create a dissociation curve that can be used to extract the off rate (Fig. 2g).

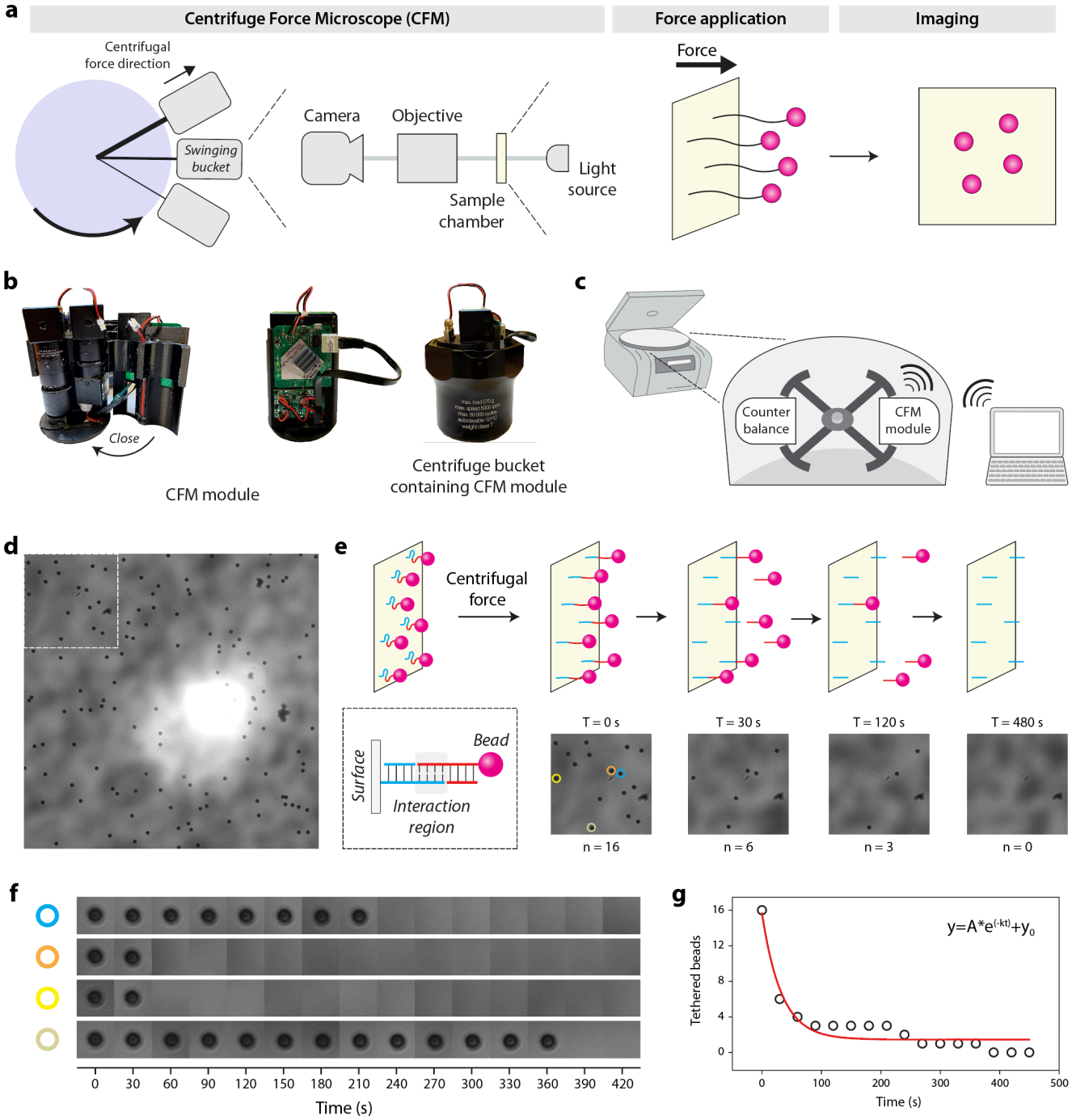

Figure 2: Concept of the Centrifuge Force Microscope (CFM) and force clamp assay. (a) The CFM is comprised of a simple video microscope that is centrifuged. Centrifugal force is applied to tethered microspheres and aligns with the imaging pathway to give a head on view of microspheres. (b) Images of the custom CFM module used in this study show the compact central optics, a clamshell style 3D printed housing, and supporting electronics, which together fit inside a centrifuge bucket. (c) The CFM module is used in a benchtop centrifuge, which is controlled by an external computer that receives a live video stream by WiFi. (d) A typical microscopy image of ~100 tethered beads at a ~40x magnification. (e) Concept and partial-frame images of tether dissociation observed in the force clamp assay. As the weak central duplex dissociates, tethered beadsfall away from the focus and disappear from view. (f) Custom MATLAB software identifies and tracks tethered beads over time and records dissociation times. Four examples shown correspond to a subset of beads in panel (e). (g) Decay plot obtained from the dissociation time analysis of the tethers in sub-frame (e). The red line is a single-exponential fit to extract off rate.

Experimental measurement of single base stacking energies

As a first test, we sought to confirm that we could measure kinetic differences between a set of DNA constructs varying by a single base stacking interaction. We designed and created three DNA constructs with short central duplexes of identical base pairs (8 bp) but varying terminal base stacking interactions (Fig. 3a and Fig. S1). In the control construct, a 3 nt poly-T spacer was used to eliminate terminal base stacking completely. Unlike most previous designs that look at pairs of base stacks or groups of pairs, this design isolates the contribution of a single base stacking interaction between two individual bases. We adopt a notation of X|Y to indicate a stacking interaction between bases X and Y read in the 5' to 3' direction. It is worth clarifying that the X resides on the 3' end of one strand and Y on the 5' of another. To realize this design in practice, we created constructs by self-assembly of the 7249 nt M13 genomic ssDNA with complementary tiling oligonucleotides, similar to our previous work with DNA nanoswitches [36,37]. The oligonucleotides tile along the length to make double stranded DNA, to provide a terminal double biotin for coupling to surfaces, and to provide "programmable" overhanging ends comprising half of the central duplex (sequences in Table S1). For the experiment, the two pairing DNA constructs were attached separately by biotin-streptavidin interactions to the microspheres and the cover glass. Within the reaction chamber, the microspheres were briefly allowed to come into contact with the cover glass to allow tethers to form, before applying force by centrifugation and measuring dissociation.

We started by probing the duplexes at forces from 5-20 pN to establish force dependent dissociation rates at room temperature (21 ± 1 °C). We hypothesized that the characteristic force scale of different constructs should be nearly identical, which would allow us to extract equilibrium energy differences from off-rates obtained at any constant force. We collected data from over 10,000 single-molecule tethers from multiple experiments that ranged from a few minutes to an hour to ensure all or nearly all beads were dissociated (Fig. 3b). The data was well described by single exponential decays to determine off-rates at different forces (Fig. S2-S4). Using the Bell-Evans model [38,39], we fit a linear trend to the logarithm of the force dependent off-rates for single A|C or A|T stacks and the no-stack control (Fig. 3c). We observed that force-dependent off rates were easily distinguishable between the constructs but followed identical slopes. This result confirmed both that individual base stacking interactions could be measured with this approach, and that the choice of force should not appreciably affect the calculated values of equilibrium free-energy of stacking. Using the 15 pN force as an example, it is clear that the three measurements are distinctly different (Fig. 3d,e), enabling the calculation of ΔG_{stack} by the ratio of off rates (Fig. 3f). We additionally verified consistency in calculated ΔG_{stack} across force values and found all results overlapping within error estimates (Fig. S5). We decided to proceed with a force of 15 pN, enabling centrifuge runs with hundreds of individual single-molecule experiments to complete in the 10-100 minutes time scale.

Having successfully proven the concept, we aimed to measure base stacking interactions between all four canonical bases (A,G,C,T) in DNA. The four bases give rise to 16 combinations, of which we considered ten unique base stacks which are T|T, C|T, A|T, G|T, C|C, A|C, G|C, A|A, G|A, and G|G. Following our validated approach, we designed DNA constructs to isolate the effect of a single base stack for all 10 combinations (Fig. S6). To accomplish this with minimal disturbance to the central duplex, we designed the central duplex to have A,C,T, and G as the 4 terminal bases. This design allowed manipulation of the strands to accomplish all of 10 combinations with only two control constructs. The list of oligonucleotides and combinations used in each construct are provided in Tables S1-S3.

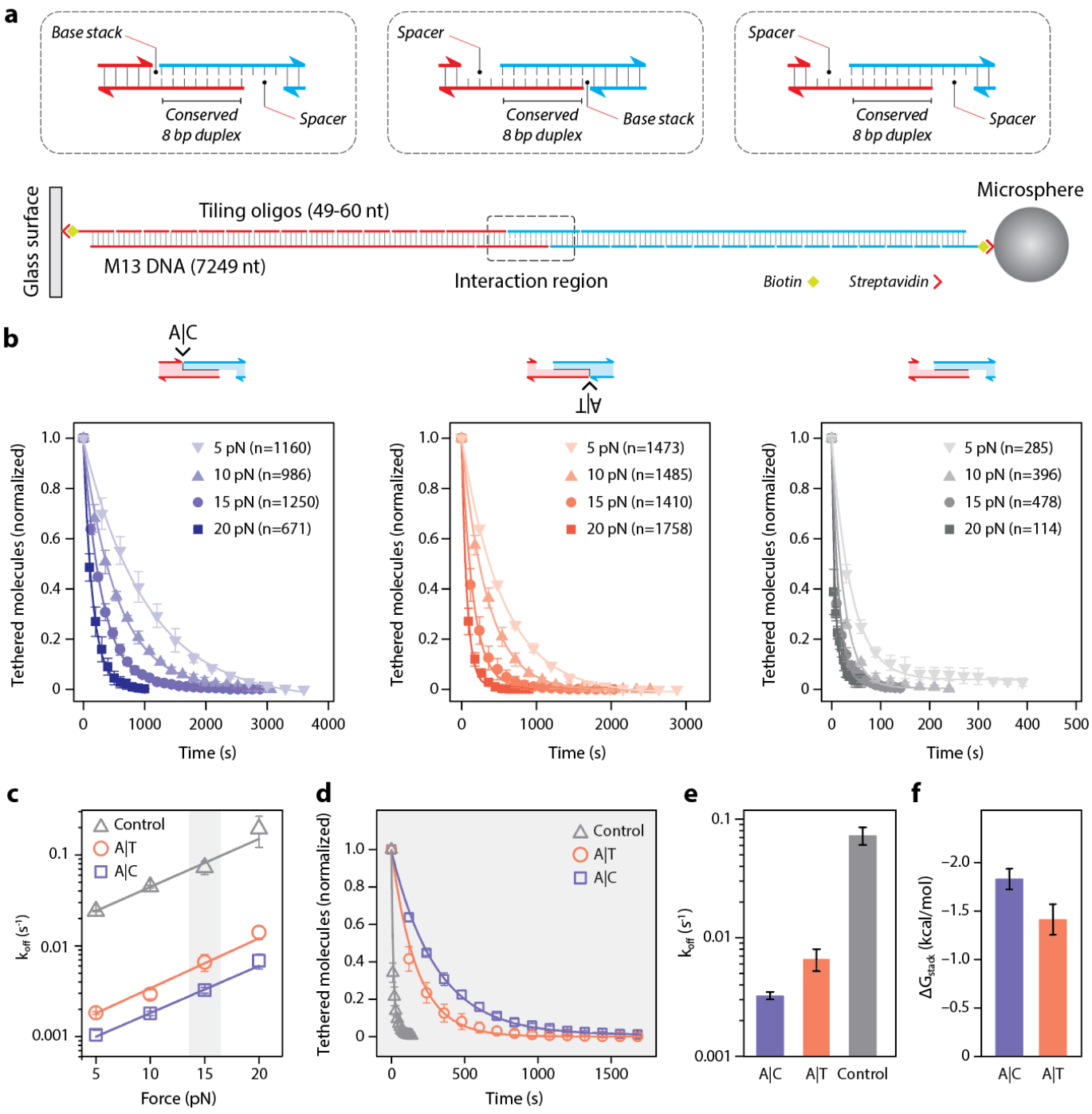

Figure 3: Experimental measurement of single base-stacking energies. (a) A weak central 8 bp duplex is designed to be flanked by a terminal base stack or no base stacks. The central interaction is formed between two DNA handles attached to a glass slide and a microsphere through biotin-streptavidin interaction. (b) Raw data and single exponential fits obtained for the A|C, A|T and control constructs at forces from 5-20 pN. Error bars represent standard deviation from at least three replicates. (c) Force-dependent off-rates fit with Bell-Evans model (solid lines) to determine thermal off-rate. Error bars represent standard deviation in off-rates from individual replicates (Figure S2-S4). (d) Analysis of the three constructs at 15 pN shows clear differences in dissociation, fit with exponential decay curves to yield off-rates (e), from which ΔG_{stack} is calculated (f).

For each construct and control, we ran experiments at 15 pN at room temperature until the large majority of the beads dissociated. Each condition was run with at least three experimental replicates, where each run also contained tens to hundreds of individual tethers. We collected and analyzed over 10,000 single molecule tethers, ranging from 171 for C|T to 2454 for G|T. From the images of each run, we measured the dissociation time for each molecule, constructed the decay plot, and found the off-rate by fitting with a single-exponential decay (Fig. 4a-b, Fig. S7-S9). We determined base stacking energies for all ten base stacks, ranging from -2.3 ± 0.2 kcal/mol for G|A (the strongest) to -0.4 ± 0.1 kcal/mol for C|T (the weakest) (Fig. 4c, Table 1). We observed a general trend that stacking energetics follows the order purine-purine > purine-pyrimidine > pyrimidine-pyrimidine. It is interesting to note that the two control constructs had nearly identical off-rates even with a 5' to 3' reversal of the central duplex.

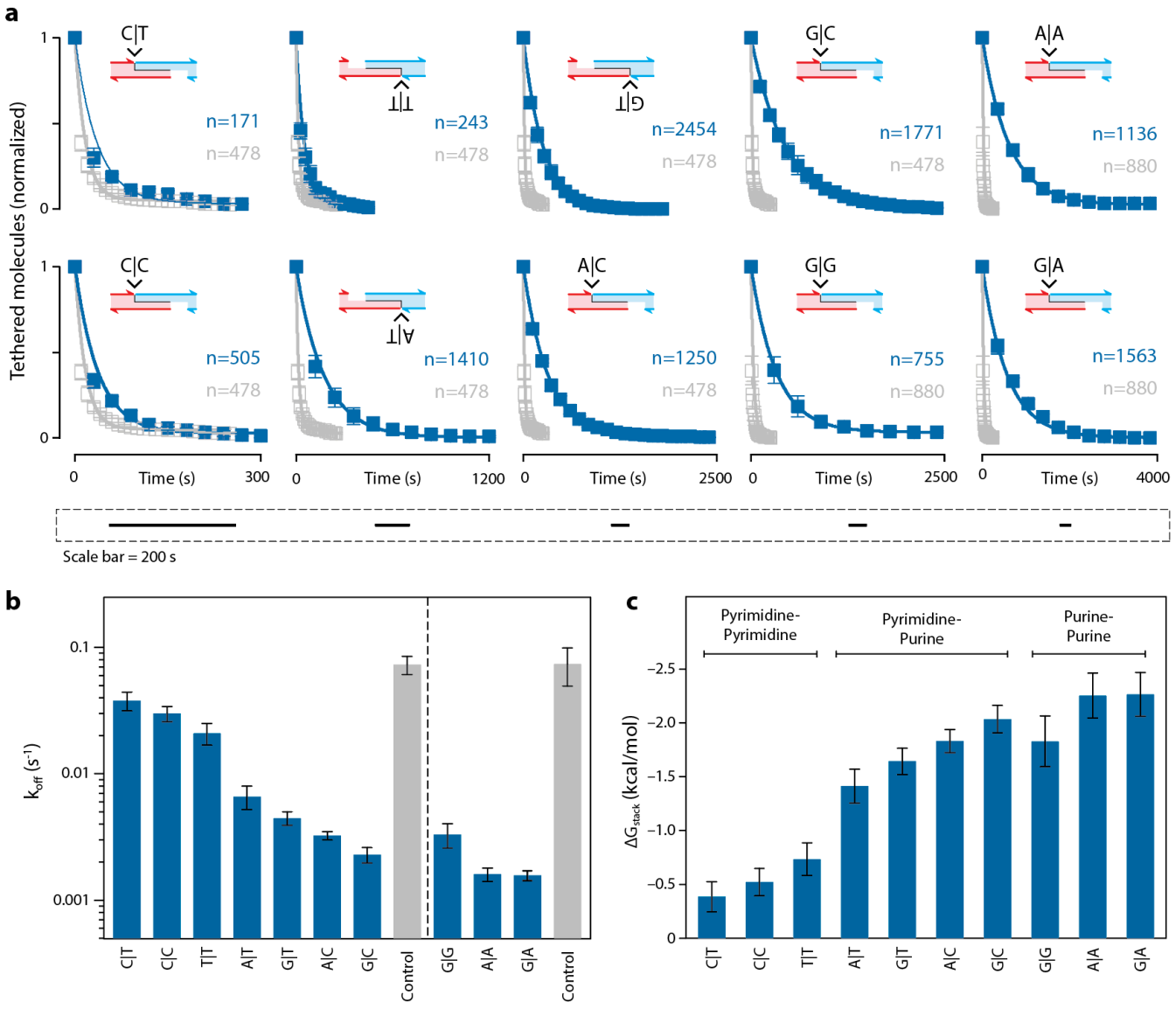

Figure 4: Comprehensive study of DNA base stacking. (a) Decay curves and single exponential fits obtained for unique base stacking combinations and their controls at a constant force of 15 pN. Error bars represent standard deviations from three data sets each consisting of one or more force clamp experiments. (b) Off-rates of DNA tethers containing various base stacks and their corresponding controls. Error bars represent standard deviation in off-rates from individual data sets (Fig. S7-S9). (c) Base stacking energies calculated from panel (b). Error bars represent calculated error propagation of results in (b).

	G|A	A|A	G|G	G|C	A|C	G|T	A|T	T|T	C|C	C|T
ΔG_{stack} (kcal/mol)	-2.3 ± 0.2	-2.3 ± 0.2	-1.8 ± 0.2	-2.0 ± 0.1	-1.8 ± 0.1	-1.6 ± 0.1	-1.4 ± 0.2	-0.7 ± 0.2	-0.5 ± 0.1	-0.4 ± 0.1

Table 1: Individual base stacking energies determined using CFM.

Influence of nucleotide modification on base stacking energy

Various chemical modifications on nucleotides can influence base stacking and base pairing energy thereby affecting the stability of nucleic acid structures [40]. We extended our approach to probe the effect of these types of modifications in comparison with canonical bases. In particular, we chose phosphorylation, methylation, fluorescein (6-FAM) and substitution of deoxyribose to ribose to study their impact on stacking on the A|C base stack (Fig. 5a). We designed modified oligonucleotides and constructed four duplexes with modified A|C stacks and individual no-stacking controls for each modification (Fig. S10). Analogous to the regular base stacking experiments, we performed 15 pN force clamps and fit decay plots to obtain the off-rates (Fig. 5b-c, Fig S11-S12) used to calculate the stacking energy of the modified A|C base stack. The control constructs were all found to be consistent within error. We observed that phosphorylation, methylation and hybrid DNA-RNA stacks are not appreciably different from the regular A|C base stack, while the bulky FAM group reduced the base-stacking energy by 0.7 ± 0.1 kcal/mol (Fig. 5d). These results show that stacking effects of chemical modifications can be measured with our technique, and suggest generally that small modifications are less likely to interfere with stacking.

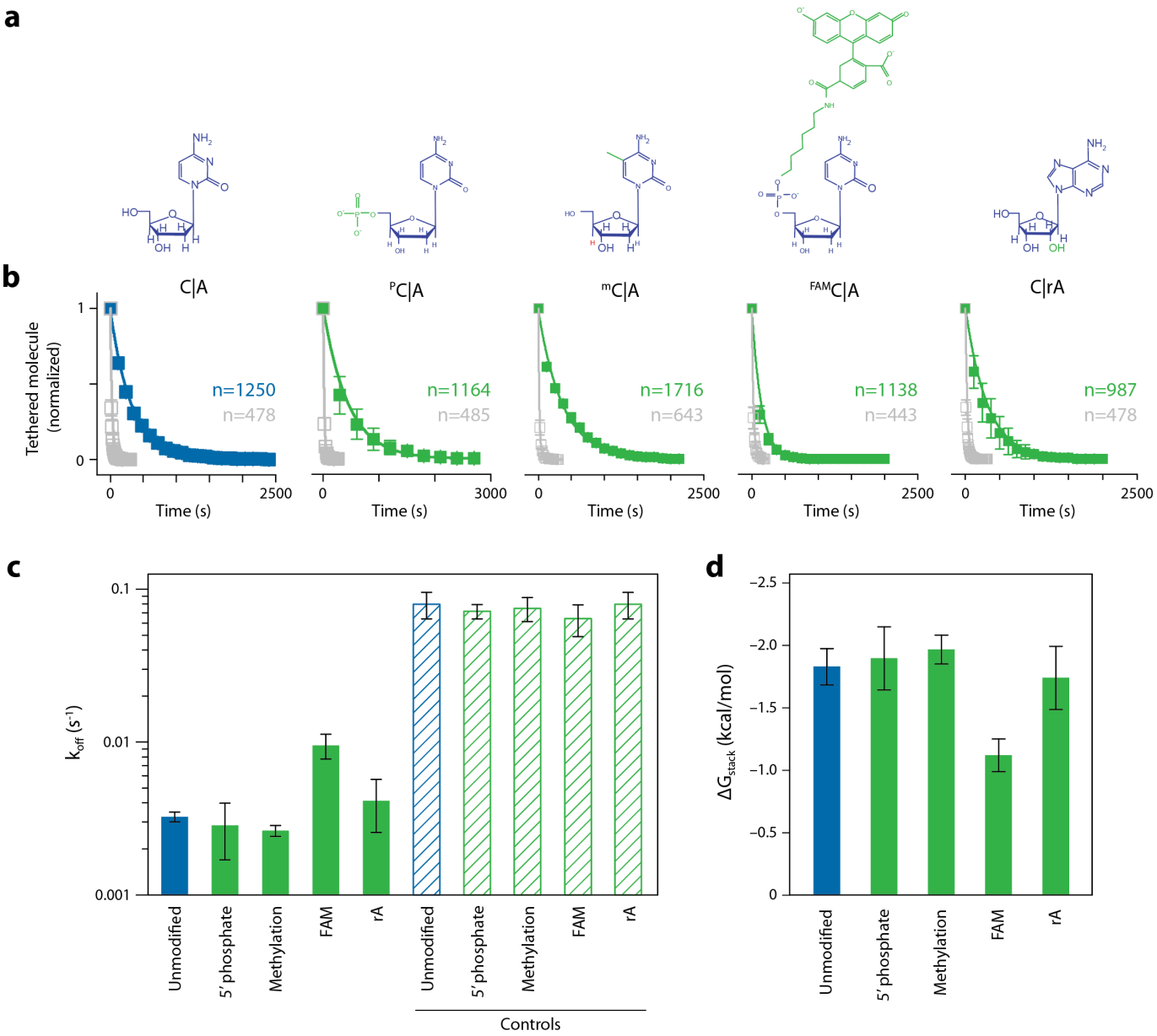

Figure 5: Effect of nucleotide modification on base stacking energy of nucleotides. (a) Modifications used in the study including 5′ Phosphorylated C, 5-methyl C, 5′ FAM modified C, 3′ ribose A. (b) Experimental data showing dissociation over time for constructs relative to their controls. Error bars represent standard deviation of triplicate data sets (c) Off-rates observed for the tethers with modified bases and their controls Error bars represent standard deviation in off-rates from individual data sets (Fig. S11-S12). (d) Free-energy of stacking calculated from off-rates in (c). Error bars represent calculated error propagation of results in (c).

Designer base-stacking to tune stability and kinetics in biotechnology applications

The elucidation of these base stacking energies can benefit many aspects of biotechnology, which often rely on forming or dynamically controlling short DNA duplexes. These include general tools in molecular biology including genetic recombination, polymerase chain reaction, and sequencing, as well as emerging technologies like gene editing, synthetic biology, and DNA nanotechnology. Of these, here we demonstrate how our results can be used in DNA nanotechnology and DNA ligation.

In DNA nanotechnology, DNA is used as a building block for nanomaterials [41] for many applications including drug delivery [42] and sensing [43]. The field relies on forming controlled contacts between short DNA segments. As a model system to test the influence of base stacking interactions, we chose the DNA

tetrahedron, a widely used structure with biosensing and drug delivery applications [18,44]. The DNA tetrahedron is hierarchically self-assembled from 3-point-star motifs, thus allowing us to modify the contacts between these motifs with different base stacks. The 3-point-star is a three-fold symmetric DNA motif consisting of three component DNA strands, a long (L), a medium (M) and a short (S) strand in a 1:3:3 ratio (Fig. 6a). Each arm of the 3-point-star motif contains two adjacent double helical domains and a strand crossover point. The double helical domains are tailed with 4-nt sticky ends that allow four such motifs to connect to each other via double cohesion to form the DNA tetrahedron. We confirmed proper assembly of the DNA tetrahedron using non-denaturing (PAGE) (Fig. 6b). We modified the double cohesion interface of the motifs to test combinations of two base stacks (G|A and A|T) in DNA tetrahedron assembly (Fig. S13). The control structure included a pair of G|A and a pair of A|T base stacks across two 4-nt sticky end connections. We modified the sequence of the component DNA strands to assemble three other versions of the DNA tetrahedron with one pair of G|A base stacks, one pair of A|T base stacks, or no base-stacks (Fig. 6c). We observed that structures containing both the G|A and A|T bases stacks were best formed, followed by the G|A structure, while the other two were apparently too weak to form stable structures (Fig. 6d, full gels in Fig. S14). To confirm that the G|A design was less stable and not just produced in a lower quantity, we tested thermal stability by incubating assembled DNA tetrahedra at 20 ºC, 30 ºC and 40 ºC for one hour. We observed a decrease in the relative stability of the structures with increased temperature, and a clear indication that the G|A structure was unstable at 40º C while the G|A + A|T structure was still intact (Fig. 6e, Fig. S14). These results are consistent with our findings that G|A base stack is stronger than A|T base stack. These experiments demonstrate the crucial role of base-stacking in the stability of DNA nanostructures, and show for the first time how changing base stacking interactions can alter stability of a DNA tetrahedron. Designing DNA nanostructures typically only involves consideration of the base pairing, and this work may point to a new dimension of control and design flexibility.

DNA ligation is a process of enzymatically joining two pieces of DNA, often facilitated by short “sticky ends” of 1-4 nt that hybridize together. Ligation is a fundamental biological process that is required for DNA repair and replication, and is integral to a wide range of biotechnology applications including sequencing, cloning, and diagnostics [45,46]. We hypothesized that modification of interfacial base stacks could alter the kinetics by changing the lifetime of the bound duplex and potentially the final efficiency of enzymatic ligation. To test this hypothesis, we designed and created short duplexes to enable ligation of products with varying sticky ends (Fig. 6f). First, we validated construction of the individual duplexes and the successful ligation of the two duplexes (Fig 6g). Next we investigated the ligation kinetics of four variants, 4 nt and 3 nt sticky ends with either T|A or G|A terminal base stacks (Fig. 6h,i and Fig. S15-S16). In the 4 nt case, we observed a slight increase in kinetics with the G|A stacks, which was most evident in the first 20 minutes of the reaction (Fig. 6j). For the 3 nt case, the difference was more striking, with a substantial difference in both the kinetics of ligation as well as the endpoint. The differences can be most clearly seen when looking at the ligated products after an 8 minute reaction, where the trend follows 4 nt G|A > 4 nt T|A > 3 nt G|A > 3 nt T|A (Fig. 6k). Interestingly, the magnitude of the change between T|A and G|A in the 3 nt case is similar to the change between 3 nt and 4 nt in G|A, suggesting that strong base stacking interactions could potentially compensate for weak base pairing in such short duplexes.

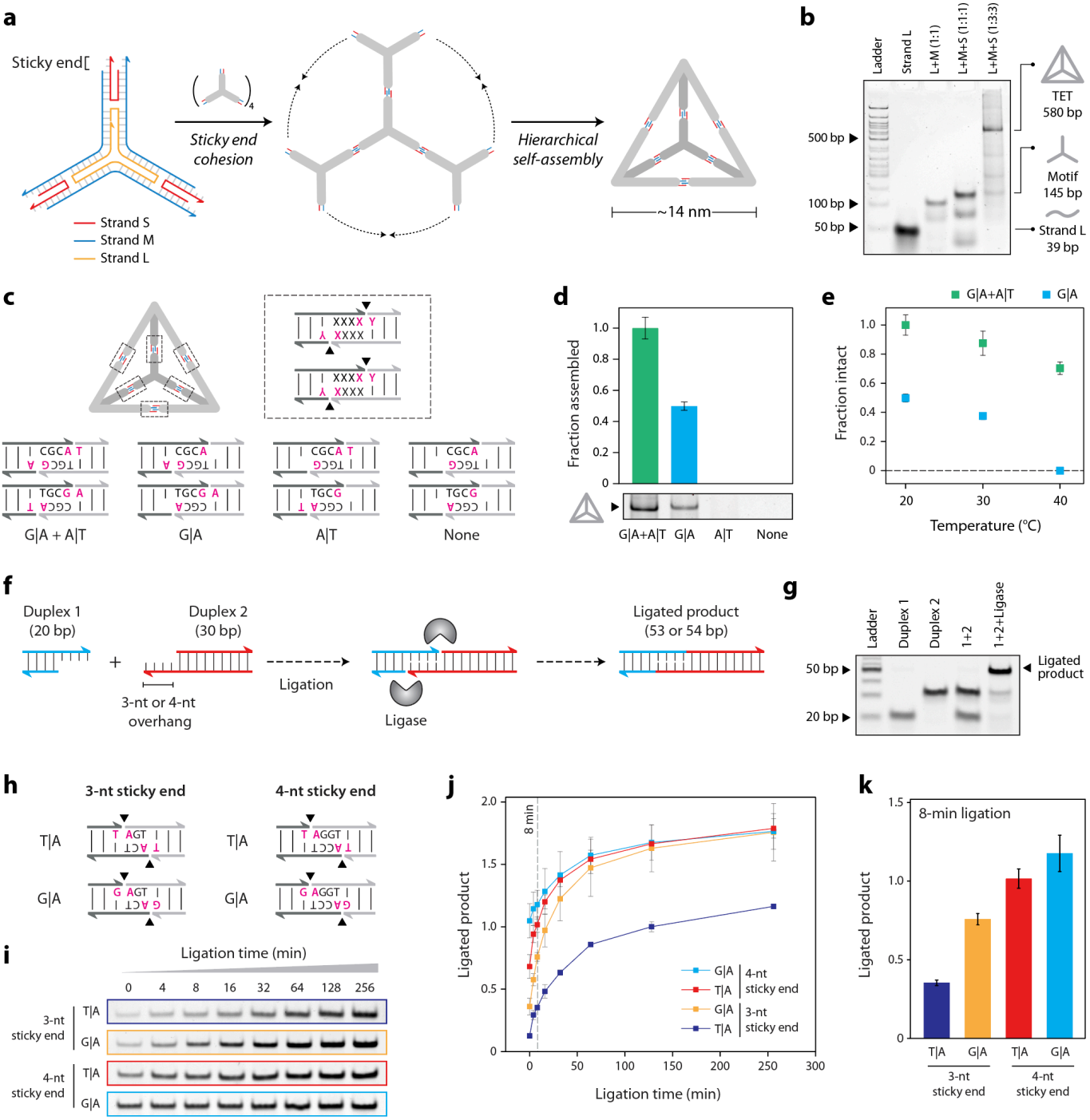

Figure 6: Designer base-stacking to tune stability and kinetics in biotechnology applications. (a) Scheme of DNA tetrahedron assembly from 3-point-star DNA motifs consisting of three component strands L, M and S. (b) Non-denaturing PAGE analysis of DNA tetrahedron assembly. (c) Modifications of base stacking interactions in DNA tetrahedra while conserving sticky end sequences. (d) Stability of DNA tetrahedra with different base stacks. (e) Thermal stability of DNA tetrahedra with various base-stacks. (f) Schematic of the ligation of two DNA duplexes with 3 or 4 base pair sticky ends. (g) Non-denaturing PAGE confirming the ligation of the two DNA duplexes. (h) Modifying base stacking interactions of sticky ends for duplexes being ligated. (i) Gel images showing the increase in band intensity of ligated fragments (full gels in Fig. S15-16). (j) Quantified ligation product over time indicates faster kinetics for duplexes with G|A base-stack compared to weaker T|A base-stack in both 4 nt and 3 nt sticky end designs. (k) Ligated product for different base stacks at 8 minutes. All error bars represent standard deviation from triplicate experiments.

Discussion

This work provides some of the most direct and comprehensive data on base stacking in nucleic acids, while also demonstrating the utility of such detailed knowledge. By employing high-throughput single-molecule experimentation using the CFM combined with novel design of DNA tethers, we measured tens of thousands of individual interations and quantified base stacking with an uncertainty of ~0.1 kcal/mol. With such small energies, measuring kinetic rates provides an inherent advantage due to the logarithmic dependence of the energies on kinetics. Single molecule techniques are a good fit for this, except they typically often can only make one measurement at a time. The CFM was developed to address limitations of throughput and accessibility in single-molecule research, and this work marks a milestone as the first large study using the CFM. To illustrate the throughput, it is worth considering the data from ~30,000 tethers we collected and typical time constants on the order of ~10 minutes would require a minimal experimental time for serial data collection on the order of ~5000 hours, as opposed to the ~200 hours of experimental time for this study. To illustrate the accessibility, we point out that these experiments were conducted largely by an undergraduate researcher, using only a low-cost CFM module in a standard benchtop centrifuge.

Our work provides important new data on base stacking energetics, which generally suggest that previous work has mostly underestimated base stacking energies. One striking example is our measurement of -2.3 kcal/mol for a single G|A stack, which is substantially more energetic than measured dinucleotide stacks containing both G|A and T|C, which were reported in the -1.0 to -1.6 kcal/mol range [25,27]. It is likely that a mix of different experimental conditions and biases in experimental designs are responsible for these differences. Our experimental approach provides a fairly direct measurement compared to some other approaches, which included extrapolating stacked/unstacked equilibrium from migration of nicked DNA in Urea gels [25], and measuring single-molecule kinetics of on and off rates in end-stacking of DNA origami tubes [27]. One recent paper published during this work used a similar construct design and found a single A|G base stack energy of -2 kcal/mol [47], consistent within error to our measurement. When we compared pairs of our measured base stacking values with previously measured dinucleotide stacks, our energies were larger in all cases by multiples ranging from 1.2 to 2.2.

The data presented here will help provide new insights into biological processes, inform DNA design in biotechnology, and improve accuracy for molecular modeling. Especially for short sticky ends that are ubiquitous in biotechnology, base stacking can play a surprisingly large role in stability. Our experimental examples of constructing DNA tetrahedra and monitoring DNA ligation provide glimpses of how our data can be used to tune DNA interactions. While our data was mostly limited to DNA base stacking, our approach can be useful for studying RNA and RNA modifications as well. Our data suggests that RNA base stacking should not be appreciably different from DNA, but further work can help clarify the role of different chemical modifications on base stacking. Our general approach can be adapted to study many variations of nucleotide interactions including those of intercalators under a variety of biologically relevant conditions.

Materials and Methods

Instrumentation

The constant force single-molecule experiments in this study were performed using a custom-built CFM, the details of which were largely reported in a previous study [32]. Briefly, the CFM consist of optics comprising a miniaturized video microscope, and of electronics allowing operation and data transmission, in an assembly that fits within a 400 mL bucket of a Sorvall X1R centrifuge. The optical components consist of a 40X plan achromatic infinity-corrected objective (Olympus) for microsphere magnification, turning mirrors (Thorlabs) for achieving required path-length and an LED with diffuser as a light source. The electronic components consists of a gigabit Ethernet machine vision camera (FLIR Blackfly Model # BFLY-PGE-50H5M-C) for imaging, a Wi-Fi router (TP-link TL-WR902AC) for wireless data transfer and communication, and a rechargeable lithium-ion battery (Adafruit) with 5V and 12V voltage step-up regulators (Pololu). These components were assembled within a 3D printed housing (Ultimaker 3). The CFM module and the centrifuge were controlled using a custom written LabVIEW program.

Sample preparation

DNA constructs were prepared by hybridizing 124 oligonucleotides (Integrated DNA Technologies) to 7249 nt single-stranded M13mp18 DNA (New England Biolabs). The construction method largely follows our approach for DNA nanoswitch construction [48]. Briefly, the M13 DNA is enzymatically linearized and then incubated with a 10 fold molar excess of backbone oligos 1-122, 150 fold overhang oligo and 500 fold stacking end oligo (Table S2) with an annealing temperature ramp from 90 ˚C to 20 ˚C. In this design, the oligo hybridized to the 3' end of the M13 DNA contains a double biotin on its 5' end for immobilization to streptavidin coated glass surface or the bead. The oligo hybridized to the 5' end of the M13 DNA extends beyond the M13, and provide a platform to anneal an oligo resulting in a 5' single-stranded overhang (Fig. S1). This overhang is used to form 'sticky-ends' for different constructs with various base stacking combinations. The list of all oligos used is given in Table S1 and combination of oligos to make constructs with different terminal bases are given in Table S2.

To immobilize DNA constructs to streptavidin coated microspheres (Thermo Fisher Dynabeads M-270 2.8 µm diameter, catalogue # 65306), we used 20 µl of streptavidin microspheres and washed thrice with 50 µl of phosphate-buffered saline containing 0.1% Tween 20 (PBST). Following the washes, the beads solution was brought to a 10 µl volume, and 10 µl of the DNA construct (~500 pM) was added to it and shaken in a vortexer at 1,400 rpm for 30 minutes. The unbound DNA and excess oligos from the construct synthesis was removed by washing the beads thrice with 50 µl PBST and resuspending in 40 µl volume.

The reaction chamber was prepared according to previous work [32]. Briefly, the reaction chamber consists of an 18 mm and a 12 mm circular microscope glass slide (Electron Microscopy Sciences, catalogue # 72230-01 & 72222-01) sandwiching two parallel strips of Kapton tape (www.kaptontape.com) creating a channel of ~ 2 mm between the glass-slides. The glass chamber is assembled on top of a SM1A6 threaded adaptor (Thorlabs). Streptavidin (Amresco) was passively adsorbed to the surface by passing 5 µl of streptavidin (0.1 mg/ml) in 1× PBS. After one minute of incubation, the chamber was washed thrice with 50 µl of PBST to remove unbound streptavidin. Next, 5 µl of DNA construct was passed through the channel and incubated for 10 minutes for the biotin-labeled DNA constructs to bind the streptavidin on the glass surface. The chamber was then washed with PBST to remove unbound constructs and excess oligos from the construct synthesis. DNA coated microspheres were passed into the chamber and incubated for 10 minutes to allow hybridization. The chamber was sealed with vacuum grease and then screwed into the CFM optical assembly until the beads are in focus.

Constant force experiment protocol

The prepared CFM with sample chamber was then loaded into the centrifuge bucket, opposite of a counterbalance with matched mass and center of mass. A custom LabView program was used to control the instrument, including the centrifuge speed, image acquisition rate, and camera parameters such as exposure time. The force generated on the tether is the centrifugal force experienced by the beads $F = m\omega^2 r$, where m is the effective mass of the bead (actual mass minus the mass of buffer displaced), ω is the angular velocity and r is the distance from the center of the rotor to the chamber (measured at 0.133 m here). The effective mass of beads was determined to be $6.9*10^{-12}$g for the Dynabeads™ M-270 (www.thermofisher.com) by previous report [29]. The RPM used were 1410, 1221, 997, and 705 for 20pn, 15pN, 10pN, and 5 pN respectively. Experiments were run at a constant force (RPM) for times up to 2 hours and data was saved as individual lossless images.

Data analysis

Force induced dissociation of the DNA tethers were measured using a previously reported MATLAB program [32]. The matlab program identifies beads using the "imfindcircles" algorithm with a user override for non-spherical, clustered beads and dirt wrongly identified as beads. Once beads are identified from an image at the start of the experiment, the software calculates the variance of the image intensity at the bead location for all the frames. When beads dissociate, it is indicated by the sharp drop in variance (i.e. high contrast to low contrast). Multiple drops in variance observed are due to break in multiple-tethered beads, which are excluded from the analysis. The decay rates were plotted in OriginLab and data was fit using single exponential decay function, $y = y_0 + A \times e^{-kt}$, where y is the fraction of tethers remaining at a given time t, y_0 is the y-axis offset or the baseline, A is the fraction of tethers at the beginning of the experiment (typically 1) and k is the off-rate for that particular force. Off-rate for any given condition was determined by at least triplicate experiments where individual k values were determined separately for each set of experiment, and data is reported as the mean and standard deviation of the replicates. The base stacking energies were extracted by comparing the off-rates, given by the equation:

$$k_{off} \propto e^{-E_a/RT} \quad \ldots\ldots(1)$$

Where, E_a is the activation energy, R is the gas constant and T is the absolute temperature. The off-rates of construct with a particular base-stack can be compared to its control construct without base stack to obtain the difference in activation energy:

$$\frac{k_{off1}}{k_{off2}} = e^{(E_{a2}-E_{a1})/RT} \quad \ldots\ldots(2)$$

The difference in activation energy between the two constructs is the energy contribution from the base stack, which can be isolated using the equation:

$$\Delta E_a = \Delta G_{Base-stack} = RT\, ln\left(\frac{k_{off1}}{k_{off2}}\right) \ldots\ldots(3)$$

where k_{off1} and k_{off2} are the off-rates of construct with and without the base stack, E_{a1} and E_{a2} are the activation energy barriers for those constructs respectively, and $\Delta G_{Base-stack}$ is the stacking energy of the interfacial bases in the non control construct.

Assembly and measurement of DNA tetrahedra

DNA tetrahedra were prepared using previously reported methods [42]. Briefly, DNA strands L, M and S (sequence are shown in Table S1) were mixed in 1:3:3 ratio at 30 nM in Tris-Acetic-EDTA-Mg^{2+} (TAE/Mg^{2+}) buffer, which contained 40 mM Tris base (pH 8.0), 20 mM acetic acid, 2 mM EDTA, and 12.5 mM magnesium acetate. The DNA solution was slowly cooled down from 95°C to room temperature over 48 hours in a water bath placed in a Styrofoam box. To assemble DNA tetrahedra with different base stacks, the following strand combinations were used:

1) Tetrahedron with both AG and AT base stacks (control): Strands L, M1, S1
2) Tetrahedron with AG base stack only: Strands L, M2, S1

3) Tetrahedron with AT base stack only: Strands L, M1, S2
4) Tetrahedron with no base stacks: Strands L, M2, S2

DNA tetrahedron assembly was validated using non-denaturing polyacrylamide gel electrophoresis. For gel analysis, 10 µl of the annealed DNA tetrahedron solution was mixed with 1 µl loading dye (containing 50% glycerol and bromophenol blue). 10 µl of this sample was loaded in each gel lane. Gels containing 4% polyacrylamide (29:1 acrylamide/bisacrylamide) were run at 4°C (100 V, constant voltage) in 1X TAE/Mg^{2+} running buffer. After electrophoresis, the gels were stained with GelRed (Sigma) and imaged using Bio-Rad Gel Doc XR+. Gel bands were quantified using ImageJ. To analyze the thermal stability of DNA tetrahedra with different base stacking combinations, we incubated the DNA tetrahedra at 30 °C and 40 °C for 1 hour. Incubated samples were prepared for gel analysis as describe above and tested using 4% PAGE. We quantified the band corresponding to the DNA tetrahedron to obtain the normalized stability levels.

DNA ligation experiments

Short duplexes with 20 and 30 bp with 3 or 4 nucleotide overhang were prepared by mixing 50µM oligos and annealing them using temperature ramp from 90 ˚C to 20 ˚C with a temperature gradiant of 1°C/min in 1X PBS buffer (see table S1). To measure the kinetics, 20 and 30 bp duplexes were mixed in equimolar ratio (0.5µM) in buffer with final concentration of 1X T4 DNA ligase buffer (NEB), 1X BSA, 1 mM ATP. 1 µl T4 DNA ligase (40 units/ µl) was added to the mixture. The reaction was terminated at the required time point by heat inactivation at 70°C for 20 mins. Then the reaction mixtures were mixed with the gel loading buffer (final concentration 1X) and were run in a 10% non-denaturing PAGE (29:1 acrylamide/bisacrylamide) at room temperature (150 V, 1hr). After electrophoresis, the gels were stained with GelRed (Sigma) and imaged using Bio-Rad Gel Doc XR+.Gel bands were quantified using ImageLabs software.

Author Contributions: The project was conceived and planned by KH and JAP, and supervised by KH. Single-molecule experiments were planned by JAP and were carried out by JAP, KT, AH, and TB. Single-molecule data analysis was performed by JAP and KT. DNA tetrahedra experiments were planned and carried out by ARC. DNA ligation experiments were planned by JAP and carried out by JAP and JV. Technical support and instrument repairs were provided by AH. The paper was written by JAP, ARC, and KH, with input from other authors.

Acknowledgements: The authors thank Andreas Karl from Thermo Fisher Scientific for providing the centrifuge main board allowing computer control. We thank Pan T.X. Li, Alan Chen, Sweta Vangaveti, and Lifeng Zhou for providing feedback on the project. Research reported in this publication was supported by the National Institutes of Health through the National Institute of General Medical Sciences under award R35GM124720 to KH.

Conflicts of Interest: The corresponding author (KH) has patents and patent applications on the CFM instrument and use, and has received licensing royalties related to those patents.

References:

[1] Orlando, L., Gilbert, M. T. P., & Willerslev, E. (2015). Reconstructing ancient genomes and epigenomes. *Nature Reviews Genetics*, *16*(7), 395-408.

[2] Li, P. T., Bustamante, C., & Tinoco, I. (2006). Unusual mechanical stability of a minimal RNA kissing complex. *Proceedings of the National Academy of Sciences*, *103*(43), 15847-15852.

[3] Chen, A. A., & García, A. E. (2012). Mechanism of enhanced mechanical stability of a minimal RNA kissing complex elucidated by nonequilibrium molecular dynamics simulations. *Proceedings of the National Academy of Sciences*, *109*(24), E1530-E1539.

[4] Stephenson, W., Asare-Okai, P. N., Chen, A. A., Keller, S., Santiago, R., Tenenbaum, S. A., ... & Li, P. T. (2013). The essential role of stacking adenines in a two-base-pair RNA kissing complex. *Journal of the American Chemical Society*, *135*(15), 5602-5611.

[5] Kool, E. T. (2001). Hydrogen bonding, base stacking, and steric effects in DNA replication. *Annual review of biophysics and biomolecular structure*, *30*(1), 1-22.

[6] Reineks, E. Z., & Berdis, A. J. (2004). Evaluating the contribution of base stacking during translesion DNA replication. *Biochemistry*, *43*(2), 393-404.

[7] Takahashi, S., Okura, H., Chilka, P., Ghosh, S., & Sugimoto, N. (2020). Molecular crowding induces primer extension by RNA polymerase through base stacking beyond Watson–Crick rules. *RSC Advances*, *10*(55), 33052-33058.

[8] Lech, C. J., Heddi, B., & Phan, A. T. (2013). Guanine base stacking in G-quadruplex nucleic acids. *Nucleic acids research*, *41*(3), 2034-2046.

[9] Abraham Punnoose, J., Ma, Y., Hoque, M. E., Cui, Y., Sasaki, S., Guo, A. H., ... & Mao, H. (2018). Random formation of G-quadruplexes in the full-length human telomere overhangs leads to a kinetic folding pattern with targetable vacant G-tracts. *Biochemistry*, *57*(51), 6946-6955.

[10] Kuruvilla, E., Schuster, G. B., & Hud, N. V. (2013). Enhanced Nonenzymatic Ligation of Homopurine Miniduplexes: Support for Greater Base Stacking in a Pre-RNA World. *ChemBioChem*, *14*(1), 45-48.

[11] Cafferty, B. J., Fialho, D. M., Khanam, J., Krishnamurthy, R., & Hud, N. V. (2016). Spontaneous formation and base pairing of plausible prebiotic nucleotides in water. *Nature communications*, *7*(1), 1-8.

[12] Chaires, J. B. (2006). A thermodynamic signature for drug–DNA binding mode. *Archives of biochemistry and biophysics*, *453*(1), 26-31.

[13] Guan, L., & Disney, M. D. (2012). Recent advances in developing small molecules targeting RNA. *ACS chemical biology*, *7*(1), 73-86.

[14] Childs-Disney, J. L., Stepniak-Konieczna, E., Tran, T., Yildirim, I., Park, H., Chen, C. Z., ... & Disney, M. D. (2013). Induction and reversal of myotonic dystrophy type 1 pre-mRNA splicing defects by small molecules. *Nature communications*, *4*(1), 1-11.

[15] You, Y., Moreira, B. G., Behlke, M. A., & Owczarzy, R. (2006). Design of LNA probes that improve mismatch discrimination. *Nucleic acids research*, *34*(8), e60-e60.

[16] Loakes, D. (2001). Survey and summary: The applications of universal DNA base analogues. *Nucleic Acids Research*, *29*(12), 2437-2447.

[17] Liu, H., Gao, J., Lynch, S. R., Saito, Y. D., Maynard, L., & Kool, E. T. (2003). A four-base paired genetic helix with expanded size. *Science*, *302*(5646), 868-871.

[18] He, Y., Ye, T., Su, M., Zhang, C., Ribbe, A. E., Jiang, W., & Mao, C. (2008). Hierarchical self-assembly of DNA into symmetric supramolecular 16olyhedral. *Nature*, *452*(7184), 198-201.

[19] Ohayon, Y. P., Hernandez, C., Chandrasekaran, A. R., Wang, X., Abdallah, H. O., Jong, M. A., … & Seeman, N. C. (2019). Designing higher resolution self-assembled 3D DNA crystals via strand terminus modifications. *Acs Nano*, *13*(7), 7957-7965.

[20] Nakata, M., Zanchetta, G., Chapman, B. D., Jones, C. D., Cross, J. O., Pindak, R., … & Clark, N. A. (2007). End-to-end stacking and liquid crystal condensation of 6–to 20–base pair DNA duplexes. *Science*, *318*(5854), 1276-1279.

[21] Wang, R., Kuzuya, A., Liu, W., & Seeman, N. C. (2010). Blunt-ended DNA stacking interactions in a 3-helix motif. *Chemical communications*, *46*(27), 4905-4907.

[22] Liu, L., Li, Y., Wang, Y., Zheng, J., & Mao, C. (2017). Regulating DNA Self-assembly by DNA–Surface Interactions. *ChemBioChem*, *18*(24), 2404-2407.

[23] Petersheim, M., & Turner, D. H. (1983). Base-stacking and base-pairing contributions to helix stability: thermodynamics of double-helix formation with CCGG, CCGGp, CCGGAp, ACCGGp, CCGGUp, and ACCGGUp. *Biochemistry*, *22*(2), 256-263.

[24] Bommarito, S., Peyret, N., & Jr, J. S. (2000). Thermodynamic parameters for DNA sequences with dangling ends. *Nucleic acids research*, *28*(9), 1929-1934.

[25] Protozanova, E., Yakovchuk, P., & Frank-Kamenetskii, M. D. (2004). Stacked–unstacked equilibrium at the nick site of DNA. *Journal of molecular biology*, *342*(3), 775-785.

[26] Yakovchuk, P., Protozanova, E., & Frank-Kamenetskii, M. D. (2006). Base-stacking and base-pairing contributions into thermal stability of the DNA double helix. *Nucleic acids research*, *34*(2), 564-574.

[27] Kilchherr, F., Wachauf, C., Pelz, B., Rief, M., Zacharias, M., & Dietz, H. (2016). Single-molecule dissection of stacking forces in DNA. *Science*, *353*(6304), aaf5508.

[28] Neuman, K. C., & Nagy, A. (2008). Single-molecule force spectroscopy: optical tweezers, magnetic tweezers and atomic force microscopy. *Nature methods*, *5*(6), 491-505.

[29] Halvorsen, K., & Wong, W. P. (2010). Massively parallel single-molecule manipulation using centrifugal force. *Biophysical journal*, *98*(11), L53-L55.

[30] Yang, D., Ward, A., Halvorsen, K., & Wong, W. P. (2016). Multiplexed single-molecule force spectroscopy using a centrifuge. *Nature communications*, *7*(1), 1-7.

[31] Hoang, T., Patel, D. S., & Halvorsen, K. (2016). A wireless centrifuge force microscope (CFM) enables multiplexed single-molecule experiments in a commercial centrifuge. *Review of Scientific Instruments*, *87*(8), 083705.

[32] Punnoose, J. A., Hayden, A., Zhou, L., & Halvorsen, K. (2020). Wi-Fi Live-Streaming Centrifuge Force Microscope for Benchtop Single-Molecule Experiments. *Biophysical journal*, *119*(11), 2231-2239.

[33] Kirkness, M. W., & Forde, N. R. (2018). Single-molecule assay for proteolytic susceptibility: force-induced collagen destabilization. *Biophysical journal*, *114*(3), 570-576.

[34] LeFevre, T. B., Bikos, D. A., Chang, C. B., & Wilking, J. N. (2021). Measuring colloid–surface interaction forces in parallel using fluorescence centrifuge force microscopy. *Soft Matter*, *17*(26), 6326-6336.

[35] Drew, H. R., Wing, R. M., Takano, T., Broka, C., Tanaka, S., Itakura, K., & Dickerson, R. E. (1981). Structure of a B-DNA dodecamer: conformation and dynamics. *Proceedings of the National Academy of Sciences*, *78*(4), 2179-2183.

[36] Halvorsen, K., Schaak, D., & Wong, W. P. (2011). Nanoengineering a single-molecule mechanical switch using DNA self-assembly. *Nanotechnology*, *22*(49), 494005.

[37] Koussa, M. A., Halvorsen, K., Ward, A., & Wong, W. P. (2015). DNA nanoswitches: a quantitative platform for gel-based biomolecular interaction analysis. *Nature methods*, *12*(2), 123-126.

[38] Bell, G. I. (1978). Models for the specific adhesion of cells to cells: a theoretical framework for adhesion mediated by reversible bonds between cell surface molecules. *Science*, *200*(4342), 618-627.

[39] Evans, E., & Ritchie, K. (1997). Dynamic strength of molecular adhesion bonds. *Biophysical journal*, *72*(4), 1541-1555.

[40] Harcourt, E. M., Kietrys, A. M., & Kool, E. T. (2017). Chemical and structural effects of base modifications in messenger RNA. *Nature*, *541*(7637), 339-346.

[41] Seeman, N. C., & Sleiman, H. F. (2017). DNA nanotechnology. *Nature Reviews Materials*, *3*(1), 1-23.

[42] Hu, Q., Li, H., Wang, L., Gu, H., & Fan, C. (2018). DNA nanotechnology-enabled drug delivery systems. *Chemical reviews*, *119*(10), 6459-6506.

[43] Xiao, M., Lai, W., Man, T., Chang, B., Li, L., Chandrasekaran, A. R., & Pei, H. (2019). Rationally engineered nucleic acid architectures for biosensing applications. *Chemical reviews*, *119*(22), 11631-11717.

[44] Chandrasekaran, A.R. & Halvorsen, K. (2019). Controlled disassembly of a DNA tetrahedron using strand displacement. *Nanoscale advances*, *1*(3), 969-972.

[45] Shuman, S. (2009). DNA ligases: progress and prospects. *Journal of Biological Chemistry*, *284*(26), 17365-17369.

[46] Tomkinson, A. E., Vijayakumar, S., Pascal, J. M., & Ellenberger, T. (2006). DNA ligases: structure, reaction mechanism, and function. *Chemical reviews*, *106*(2), 687-699.

[47] Rieu, M., Vieille, T., Radou, G., Jeanneret, R., Ruiz-Gutierrez, N., Ducos, B., … & Croquette, V. (2021). Parallel, linear, and subnanometric 3D tracking of microparticles with Stereo Darkfield Interferometry. *Science Advances*, *7*(6), eabe3902.

[48] Chandrasekaran, A. R., Dey, B. K., & Halvorsen, K. (2020). How to Perform miRacles: A Step-by-Step microRNA Detection Protocol Using DNA Nanoswitches. *Current protocols in molecular biology*, *130*(1), e114.